Enabling harmonic balance method to be applied for distributed geometric nonlinearities in structural dynamics

S. Lian, F. El Haddad, L. Salles
Department of Mechanical Engineering, Imperial College London
London, SW6 2AZ, UK
e-mail: **s.lian17@imperial.ac.uk**

Abstract
In this paper, a general harmonic balance finite element method is developed for the 3D structure. An investigation of the nonlinear dynamic behavior of a three dimensional beam due to distributed geometric nonlinearities arising from large displacements is proposed in this paper. Green-Lagrange strain measures paired with the Harmonic Balance Method with Alternating Frequency/Time (HB-AFT) domain technique to simulate the nonlinear response has been used to obtain the dynamic behaviours for both the linear and nonlinear cases. It has been found that geometric nonlinearities present hardening effects on the forced frequency response of the system. Also, higher order elements have shown to better capture the vibration characteristics of the structure, however this comes with a cost of increased computational time.

1 Introduction

In the last couple of decades global awareness of climate change and economic impact of high fuel consumption and low propulsion efficiency in the aviation industry has led to major changes in manufacturing practices all the way up to the design stages. Aero-engines to attain high fuel efficiencies require sustained operations at increasingly higher temperature using lightweight materials. This poses a structural integrity challenge from a vibration analysis standpoint whereby components become ever more sensitive to fatigue failure and structural instabilities. From a cost perspective the ability to simulate dynamic vibration behaviors at the design stage can reduce the cost of expensive prototyping and testing, as well as enabling simulation of high rotational speeds, dynamic loads, and rotor-dynamic effects [1] which would be difficult to test otherwise. Therefore, the ability to model accurately dynamic nonlinear behaviors becomes imperative in the vibration analysis of safe-critical components. Nonlinear systems are those for which the principle of superposition does not hold due to the coupling of modes, internal resonance and shifting of natural frequencies. Main sources of nonlinearities derive from frictional forces, material and geometrical nonlinearities. Geometrical nonlinearities in particular arise due to large displacements and solid rotations and thus the nonlinear strain-displacements relations [2].

This paper will focus on the analysis of dynamic nonlinear behavior of geometric nonlinearities using forced frequency response on a 3D beam using Green-Lagrange strain measures and Harmonic Balance Method (HBM). HBM is the most popular frequency domain method used for calculating the periodic steady-state response. It was first introduced by Krylov and Bogoliubov [3] while Urabe introduced the method for Fourier approximations truncated to several harmonics into the harmonic balance in 1960s [4] also employed in other studies [5]. HBM has also been coupled with alternating Fourier transformation (AFT) by Cameron in 1989 [6] which considerably improved the HBM method. The AFT methodology computes the nonlinear term in time domain and then transfers it to the frequency domain, providing better approximation than the analytical description of nonlinear term in frequency domain. The investigation herein will make use of the AFT enhanced HBM method to numerically solve the dynamic equation of motion of the beam. Other

studies [7] have made use of the finite difference method to investigate free vibrations of clamped and simply supported thin plates which showed that the solution of the natural frequency is more accurate when using a higher number of sub-domains. Attempts at improving the finite difference for the vibration analysis of rotating turbomachinery blades have made use of smaller matrix leading to faster convergence time compared to the first order method [8].

Other time domain numerical techniques for predicting the nonlinear behaviour of systems such as the shooting and Poincaré method [9] have been surveyed and reviewed over time by Keller and Meyer [10]-[11]. The shooting method in particular has proven to be particularly useful to solve boundary problems for ordinary differential equations (ODEs). Pai and Palazotto [12] used multiple shooting method to investigate flexible beams undergoing large elastic rotations and displacements in three-dimensional space in a two point boundary problem to assess the performance of nonlinear finite-element codes in analyzing large structural deformations. Studies conducted on nonlinear free vibrational of double-clamped beams subjected to axial loads have used modified Lindstedt-Poincare methods to obtain analytical expression of natural frequencies as a function of beam axial load and slenderness ratio [13]. Chen et al [14] also employed the multidimensional Lindstedt–Poincare (MDLP) to investigate nonlinear vibration of axially moving systems showing that the MDLP method agree reasonably well with that obtained by the incremental harmonic balance (IHB) method.

The nonlinear dynamic response of a long slender beam has been the subject of many theoretical and experimental efforts due to the fact that engineering safe-critical components like turbine blades and aircraft wings can be modelled as a beam-like slender structure. Euler-Bernoulli beam theory has been used extensively to analyse small deformation of slender beam under load [15]. Yoon et al investigated simply supported double cracked beam modelled using the Euler-Bernoulli theory [16] to identify the influence of crack depth and position on natural frequency and vibration mode. In order to account for shear strain and stresses variation over the cross section of a beam, Timoshenko beam theory provides a better approximation of the beam deformation [17][18]. However, Euler-Bernoulli and Timoshenko inherently have great limitations in a full mechanical analysis as only 2D beam elements can be used while most structure investigated will be three-dimensional.

The finite element method (FEM) analysis carried out in this paper therefore uses three-dimensional brick elements which model the nonlinear hyper-elastic formulation of the beam. A clear advantage of using the FEM analysis is that all matrices in the equation of motion are characterized by high degree of sparsity (i.e. large number of zero elements as its entries). Since the computational requirements to analyse complex engineering structures can easily become unmanageable, FEM provides a memory efficient computational approach to investigate nonlinear behavior. In the investigation herein presented the high level of sparsity gives us the choice to use Compressed Sparse Row (CSR) storage numerical method to reduce the computational burden to converge to a solution. Other studies [19]-[20] in blade vibration monitoring have focused on the utilisation of the CSR method to develop models to reconstruct the under-sampled blade tip-timing (BTT) signals in order to build unknown multi-mode blade vibrations.

Green-Lagrangian strain measures are widely used in the vibration analysis of different structures. Studies [21]-[22] employed a Green-Lagrangian framework to analyse the free vibration of composite laminate plates in higher order shear deformation theory. Almansi-Lagrange strain commonly used in the Updated Lagrangian formulation have been shown to provide good agreement in the context of modelling and simulation of damage in large deformations in elastomers [23].

The objective of this research is to investigate the dynamic behavior of a beam undergoing forced frequency response including geometric nonlinearities due to large deformation. The model will use 3D solid brick element formulation paired with the Green-Lagrange strain framework and the Harmonic Balance Method. Algorithms used in the numerical analysis are highlighted in section 2. Finite element model used for the simulations is illustrated in section 3.1. The numerical results are discussed in section 3. Final conclusions and future outlooks are drawn up in section 4.

2 Governing Equations

2.1 Green-Lagrangian Strain

Strain is a measure for the non-rigid part of the deformation. When undergoing a geometrically nonlinear deformation process, continuum bodies will exhibit large strains. Green-Lagrange strain measures, E_{ij}, are employed in this paper to describe the nonlinear geometric effect for structures undergo finite deformation. The explicit expression of the tensor is shown in Equation 1.

$$E_{ij} = \frac{1}{2}\left(\frac{\partial u_i}{\partial X_i} + \frac{\partial u_j}{\partial X_j} + \frac{\partial u_k}{\partial X_i}\frac{\partial u_k}{\partial X_j}\right) \tag{1}$$

In Green-Lagrangian deformation tensor, partial derivative of the displacement vector **u** are with respect to the material/reference coordinates **X**, i.e. the coordinate system of the undeformed configuration. This strain measure is independent of rigid body rotations, which makes it suitable for describing strain in engine blades.

Linear 3D Saint Venant–Kirchhoff material law (Equation 2) is used in this paper for the constitutive relationship of the material and derivation of stress measure [24],[25]. **S** represents the second Piola-Kirchoff stress tensor, μ and λ are the Lamé constants.

$$\mathbf{S} = \lambda \operatorname{tr}(\mathbf{E})\,\mathbf{I} + 2\mu\mathbf{E} \tag{2}$$

2.2 Finite Element Method

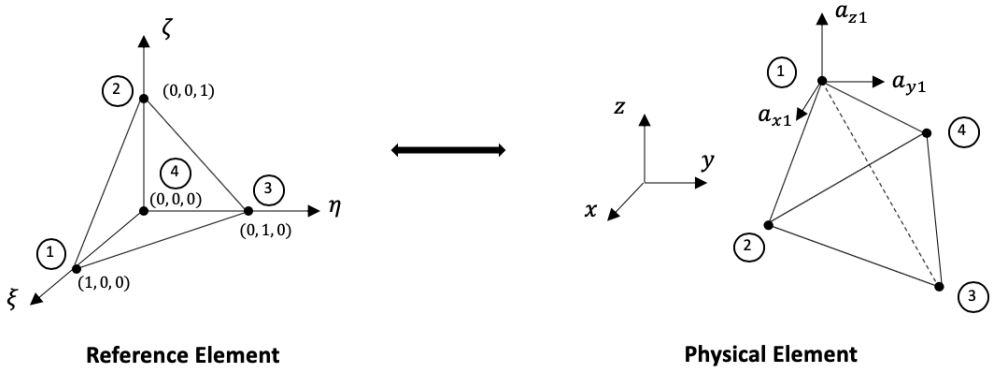

Figure 1: Transformation between physical and reference element.

In finite element analysis, the structure is assigned with a set of node points associated with given number of Degree-of-Freedoms (DOFs). The region confined by the adjacent nodes is referred to as an element [26]. In 3D solid element, nodes are allowed to translate along the x, y, z axes, hence each node has 3 DOFs. The estimated displacement vector **u** of each element can be defined as in Equation 3, where **N** is the shape function matrix, $\mathbf{a}_e$ is the column vector of nodal displacement. n stands for the total number of nodes in the element and subscript e refers to elementary quantities. For the convenience of computation, physical elements are all transformed into reference element as shown in Figure 1, shape functions of the reference element with coordinates (ξ, η, ζ) are used.

$$\begin{aligned}\mathbf{u}_e(\xi,\eta,\zeta) &= \begin{Bmatrix} u_x & u_y & u_z \end{Bmatrix}^{\mathsf{T}} = \mathbf{N}(\xi,\eta,\zeta)\cdot\mathbf{a}_e(t)\\ \mathbf{a}_e &= \begin{Bmatrix} a_{x1} & a_{y1} & a_{z1} & a_{x2} & a_{y2} & a_{z2} & \dots & a_{xn} & a_{yn} & a_{zn} \end{Bmatrix}^{\mathsf{T}}\end{aligned} \tag{3}$$

Green strain vector $\boldsymbol{\epsilon}$ (Equation 4) can be decomposed into linear part $\boldsymbol{\epsilon}_0$ and nonlinear part $\boldsymbol{\epsilon}_1$. Details of the shape function matrix **N** and matrices of derivatives of the shape function $\mathbf{B}_0$ and $\mathbf{B}_1$ can be found in

Appendix A.

$$\begin{aligned}\boldsymbol{\epsilon} &= \boldsymbol{\epsilon}_0 + \boldsymbol{\epsilon}_1 \\ &= \mathbf{B}_0\left(\xi,\eta,\zeta\right)\cdot\mathbf{a}_e + \frac{1}{2}\cdot\mathbf{B}_1\left(\mathbf{u}\right)\cdot\mathbf{a}_e\end{aligned} \tag{4}$$

2.3 Equation of Motion

$$[\mathbf{M}]\left\{\ddot{\mathbf{x}}(t)\right\} + [\mathbf{C}]\left\{\dot{\mathbf{x}}(t)\right\} + [\mathbf{K}(\mathbf{x})]\left\{\mathbf{x}(t)\right\} = \left\{\mathbf{F}_{ext}(\omega,t)\right\} \tag{5}$$

$$[\mathbf{M}]\left\{\ddot{\mathbf{x}}(t)\right\} + [\mathbf{C}]\left\{\dot{\mathbf{x}}(t)\right\} + [\mathbf{K}_0]\left\{\mathbf{x}(t)\right\} + \left\{\mathbf{F}_{nl}(\mathbf{x},t)\right\} = \left\{\mathbf{F}_{ext}(\omega,t)\right\} \tag{6}$$

The matrix format of equation of motion (Equation 5) can be achieved by applying Euler–Lagrange equation on to the energy expressions of the system. **M**, **C**, **K** represents the mass, damping and total stiffness matrix respectively, **x** is a vector listing the displacement in x, y, z directions of each node and $\mathbf{F}_{ext}$ represents the periodic excitation force vector with frequency ω. The dots refer to the derivatives with respect to time t. Damping matrix is considered as a proportion of the mass matrix, i.e. $\mathbf{C} = \alpha\,\mathbf{M}$. Expressions of the mass and stiffness matrix are displayed in Equation 7 and 8. **D** is the constitutive matrix based on linear Saint Venant–Kirchhoff law (Equation 2). The total stiffness matrix **K** can be decomposed into $\mathbf{K}_0$ and $\mathbf{K}_{nl}$, where $\mathbf{K}_{nl}$ includes all the terms with $\mathbf{B}_1$, hence forms the nonlinear force vector $\mathbf{F}_{nl}$ of the dynamic system in Equation 6.

$$\begin{aligned}[\mathbf{M}] &= \int \mathbf{N}^{\intercal}\left(x,y,z\right)\rho\,\mathbf{N}\left(x,y,z\right)\mathrm{d}\,\Omega \\ &= \sum_{i=1}^{N}\mathbf{N}^{\intercal}\left(\xi_i,\eta_i,\zeta_i\right)\rho\,\mathbf{N}\left(\xi_i,\eta_i,\zeta_i\right)\cdot\left|\mathrm{Jac}\left(\xi_i,\eta_i,\zeta_i\right)\right|\cdot w_i\end{aligned} \tag{7}$$

$$\begin{aligned}[\mathbf{K}] &= \int\left[\mathbf{B}_0+\mathbf{B}_1(\mathbf{u})\right]^{\intercal}\cdot\mathbf{D}\cdot\left[\mathbf{B}_0+\frac{1}{2}\mathbf{B}_1(\mathbf{u})\right]\mathrm{d}\,\Omega \\ &= \sum_{i=1}^{N}\left[\mathbf{B}_0+\mathbf{B}_1(\mathbf{u})\right]^{\intercal}\cdot\mathbf{D}\cdot\left[\mathbf{B}_0+\frac{1}{2}\mathbf{B}_1(\mathbf{u})\right]\cdot\left|\mathrm{Jac}\left(\xi_i,\eta_i,\zeta_i\right)\right|\cdot w_i \\ &= [\mathbf{K}_0]+[\mathbf{K}_{nl}(\mathbf{u})]\end{aligned} \tag{8}$$

The integral functions can be estimated by employing Gaussian quadrature rule. N is the total number of Gaussian Quadrature points, ξ_i, η_i, ζ_i are the quadrature points and w_i is the corresponding quadrature weight.

2.4 Harmonic Balance Method with Alternating Fourier Transformation

The nonlinear ODE involved in the dynamic systems (Equation 6) can be solved by using harmonic balance method with alternating Fourier transformation. HBM uses a linear combination of sinusoids to build the solution. The response $\mathbf{x}(t)$ to the periodic excitation is expected to be ω-periodic. The periodic vectors **x**, $\mathbf{F}_{ext}$ and $\mathbf{F}_{nl}$ in Equation 6 can be estimated as a truncated Fourier series to the N_H-th harmonic as shown in Equation 9. $\tilde{\chi}(t)$ represents the ω-periodic vectors. $\tilde{\chi}$ is the collection of all Fourier coefficients for all DoFs in the system.

$$\chi(\omega,t) = \frac{1}{2}\tilde{\chi}^{0,c} + \sum_{n=1}^{N_H}\tilde{\chi}^{n,c}\cos(n\omega t) + \tilde{\chi}^{n,s}\sin(n\omega t) \tag{9}$$

$$\tilde{\chi} = \begin{bmatrix}\tilde{\chi}^{0,c} & \tilde{\chi}^{1,c} & \tilde{\chi}^{1,s} & \tilde{\chi}^{2,c} & \tilde{\chi}^{2,s} & \ldots & \tilde{\chi}^{N_H,c} & \tilde{\chi}^{N_H,s}\end{bmatrix} \tag{10}$$

The equation of motion in time domain (Equation 6) can hence be transformed into Equation 11, where $\tilde{\cdot}$ denotes parameter in frequency domain and $\mathbf{A}(\omega)$ describing all the linear dynamics part of the system. Details of $\mathbf{A}(\omega)$ can be found in Appendix B. Parameters $\tilde{\mathbf{q}}$, $\tilde{\mathbf{b}}_{nl}$ and $\tilde{\mathbf{b}}_{ext}$ are $\mathbf{x}$, $\mathbf{F}_{nl}$ and $\mathbf{F}_{ext}$ in frequency domain respectively. Newton–Raphson method [27] is used to solve the harmonic balance equation $\mathbf{Z}(\omega, \tilde{\mathbf{q}})$.

$$\mathbf{Z}(\omega, \tilde{\mathbf{q}}) \equiv \mathbf{A}(\omega)\tilde{\mathbf{q}} + \tilde{\mathbf{b}}_{nl}(\tilde{\mathbf{q}}) - \tilde{\mathbf{b}}_{ext} = 0 \tag{11}$$

$$\tilde{\mathbf{q}} \xrightarrow{\text{IDFT}} \mathbf{x}(t) \xrightarrow{\mathbf{K}_{nl}(\mathbf{x})} \mathbf{F}_{nl}(\mathbf{x}) \xrightarrow{\text{DFT}} \tilde{\mathbf{b}}_{nl}(\tilde{\mathbf{q}}) \tag{12}$$

Alternating frequency-time domain (AFT) method is used to compute $\tilde{\mathbf{b}}_{nl}$. Solution $\tilde{\mathbf{q}}$ at each Newton–Raphson iteration is transformed into time domain by applying Inverse Discrete Fourier Transform (IDFT). Discrete Fourier Transform (DFT) is then followed to compute the resulting nonlinear force in frequency domain $\tilde{\mathbf{b}}_{nl}$ as shown in Equation 12.

2.5 Continuation Scheme

Studying the evolution of periodic solutions $\mathbf{x}$ with respect to the frequency ω of the harmonic forcing $\mathbf{F}_{ext}$ can be very useful. Continuation scheme provides algorithmic procedures to generate a continuum of periodic solution $\mathbf{x}$. Continuation algorithms are based on two main steps applied recursively for each point in the state-control space $(\mathbf{x}, \omega)$. A prediction point is guessed first based on the previous obtained points, then follows a correction step which provides the new point in the state-control space. The path following procedure in continuation scheme is an useful theoretical tool to track the turning path of the solutions and find coexisting solutions for the same parameter value in many applications due to its versatility and robustness. Secant method and arc length constraint are chosen to be the prediction and correction method respectively for the continuation scheme in this paper. Details on the continuation scheme employed in this paper can be seen in Appendix B.

3 Numerical Results

3.1 Model Description

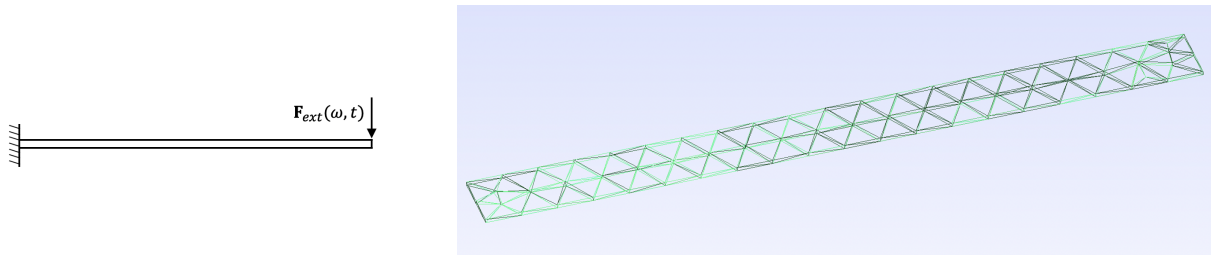

(a) Schematic Model (b) FEM mesh with 3D tetrahedron solid elements

Figure 2: 3D cantilevered beam model used for numerical analysis.

In this paper, a 3D cantilevered beam model with dimension of $5\text{mm} * 100\text{mm} * 1000\text{mm}$ is used. The periodic excitation force is applied at the free end of the beam (Figure 2a). The nonlinear beam used in is made with homogeneous material of Young's Modulus $E = 104$ GPa and density $\rho = 4400\ \text{kg/m}^3$. Parameter α involved in the damping matrix is chosen to be $\alpha = 0.01 * \omega_0$, where ω_n is the natural frequency of the cantilevered beam. 3D tetrahedron solid elements are used in the FE model (Figure 2b). The mesh studied in this paper has 277 elements in total.

3.2 Static Analysis of Nonlinear Beam

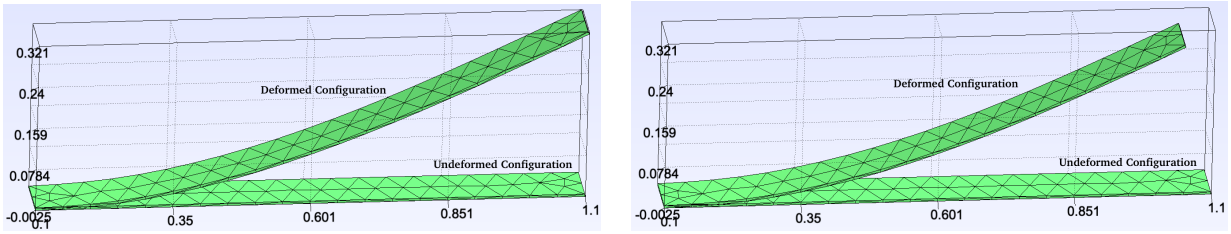

(a) Linear Model (b) Nonlinear Model

Figure 3: Deformation of 3D cantilevered beam under static point load.

Figure 3 shows the deformation of the 3D cantilevered beam under static point load $\mathbf{F}_{ext} = 10^4$ N. Four nodes tetrahedron elements are used in the FE model. Figure 3a shows the deformation of the 3D beam with consideration of only the linear part of the strain $\boldsymbol{\epsilon}_0$ (Equation 4), artifacts can be observed such as increase in volume. Figure 3b shows the simulation result with the full Green-Lagrange strain measure employed in the model. The effect of the nonlinear part of the strain measure becomes significant when undergoing large deformation, hence linear approximation is no longer accurate enough when modeling the system.

3.3 Dynamic Analysis of Nonlinear Beam

3.3.1 Forced Frequency Response

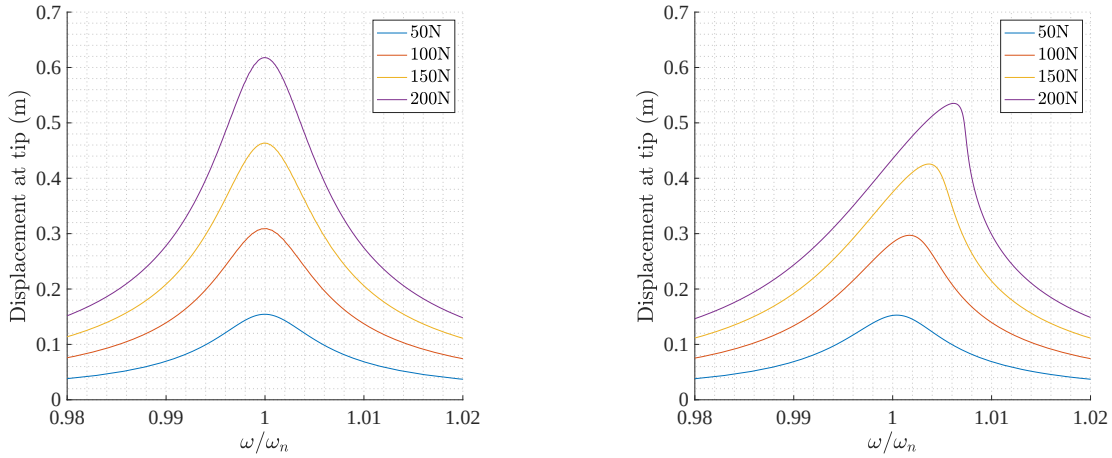

(a) Linear FRF (b) Nonlinear FRF

Figure 4: Forced frequency response of 3D cantilevered beam under periodic point load.

Figure 4 shows the forced frequency response of the first bending mode of the cantilevered beam under different level of periodic excitation force. $N_H = 5$ and linear 4 nodes tetrahedron elements are employed. Frequency is scalded by the natural frequency of the structure $\omega_n = 38.872$ Hz. Hardening effects of the nonlinear strain can be observed from the FRF plot in Figure 4b.

Resonance frequencies and the mode shapes of the model can be computed by solving the eigenproblem in Equation 13, where ω is the vector containing all the resonance frequencies and Φ is the matrix listing all the corresponding mode shapes. Table 1 shows the comparison of the first three lowest resonance frequencies yields by using different element type with the analytical values. 'Tet 4' indicates the 4 nodes linear

tetrahedron element with nodes at the corners only as shown in Figure 1 and 'Tet 10' indicates the 10 nodes quadratic tetrahedron element with 6 more nodes at the mid of the edges. Same mesh (Figure 2b) but different element type are used. The analytical values are calculated by following the formula in [28]. For the same level of mesh resolution, quadratic elements show much better convergence and produce much more accurate results than the linear elements. 20 nodes hexahedron elements (another commonly used 3D solid element) are also investigated, indicated as 'Hex20' in the table. A much fewer elements are used to generate the mesh for the cantilevered beam. The results show that quadratic elements have a much better capability to capture curvature than linear elements. However the computational time is increased due to the increase in total DoFs and increase in Gaussian Quadrature points when computing matrices (Equation 7-8).

$$\left[\mathbf{K}_0 - \omega^2 \mathbf{M}\right] \Phi = 0 \tag{13}$$

Table 1: Comparison of resonance frequencies computed by different element types.

	Tet 4	Tet 10	Hex 20	Analytical
No. of elements	277	277	13	N/A
ω_1	38.872	4.201	4.018	3.926
ω_2	100.139	27.358	25.307	24.607
ω_3	236.665	81.928	71.797	68.910

3.3.2 Computational Time

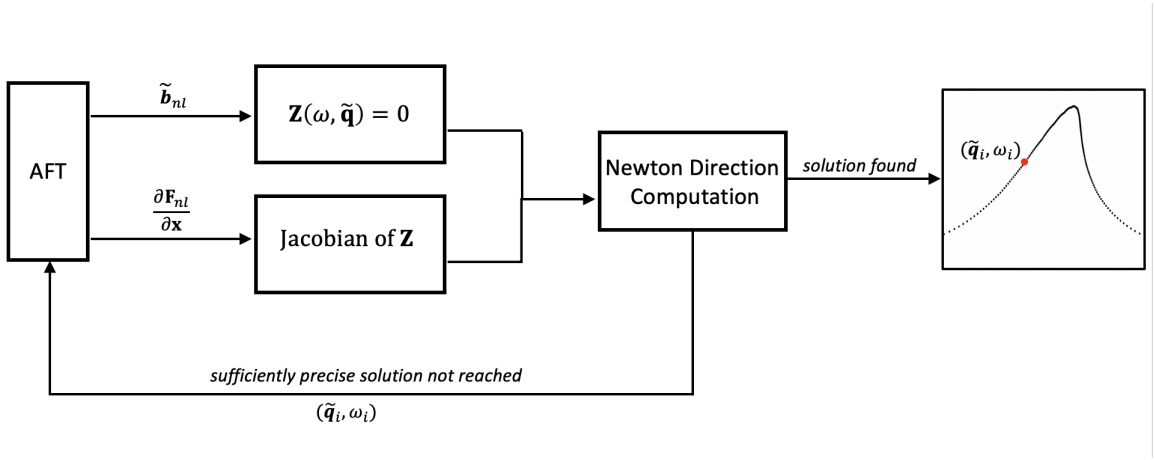

Figure 5: Flowchart for the dynamic analysis of the structure.

Figure 5 depicts the procedures involved when generating the points on the nonlinear FRF plot. Details of algorithms used in Newton direction computation for harmonic balance can be found in Appendix C. Figure 6 shows the computational time consumed by different stages when generating Figure 4b with excitation force at an amplitude of 200 N. AFT takes the majority of the computational time, this is due to the calculation of $\mathbf{F}_{nl}$ and the corresponding Jacobin matrix $\partial \mathbf{F}_{nl}/\partial \mathbf{x}$ at each time step and transformation from time domain into frequency domain. 2^8 time steps are used in the IDFT and DFT steps in Equation 12. Matrices generated by FEM have high sparsity level, CSR (Compressed Sparse Row) format is hence selected to store the matrices. Intel MKL Pardiso solver is used for applying the Newton direction computation to solve Equation 11 in sparse matrices. Sparse matrix solver and the assembly of Jacobin matrix for Newton direction computation ranks second and third respectively in the computational time consumed. Computation of $\mathbf{Z}(\omega, \tilde{\mathbf{q}})$ by manipulating the sparse matrices is efficient and takes negligible time. The peaks on the plot are corresponding to the increase in the iteration numbers when solving the equations. Computational times

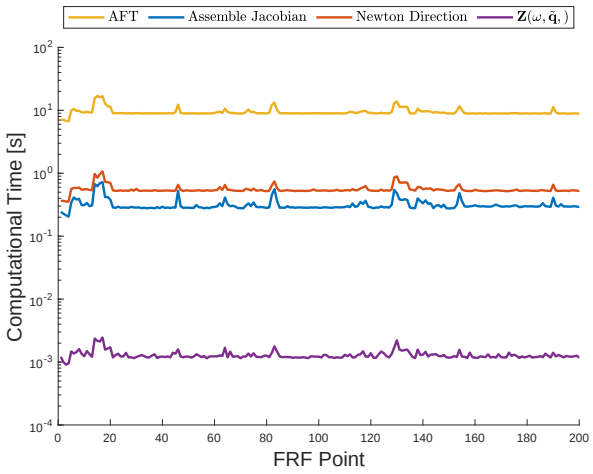

Figure 6: Computational time for each point on FRF plot with $\mathbf{F}_{ext} = 200\sin(\omega t)$.

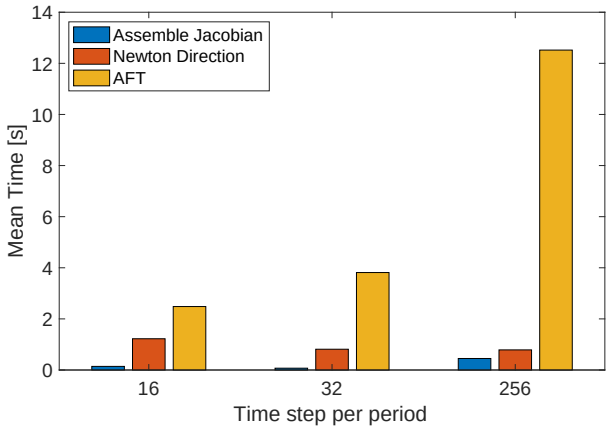

Figure 7: Comparison of computational time with different time steps per period.

arising from different time steps per period used in DFT and IDFT are shown in Figure 7. Mean time taken by the most computational consuming procedures are compared. AFT is the most sensitive procedure to the time steps per period. Linear 4 nodes tetrahedron elements are used in this study. Higher order elements can increase the accuracy of the result however the increase in the total DOFs in the system and number of Gaussian points used for constructing matrices (Equation 7 and 8) will cause the increase in the overall computation time.

4 Conclusion and Outlook

Investigation of the nonlinear behavior of the dynamic response of a 3D beam using the AFT Harmonic Balance Method within the Green-Lagrange strain framework has been presented in this paper. In particular it has been shown that when structures undergo large deformation, linear approximations are no longer sufficient to produce accurate solution for the response of the structure.

The Harmonic balance method with alternating frequency-time domain method has been shown to be an effective mathematical tool for calculating the steady-state nonlinear dynamic solution. Geometric nonlinearities show hardening effects on the forced frequency response of the system.

Finally, to accurately capture the complex curvatures, higher order elements are preferred, however this comes with a cost of increased computational time.

Reduced order modelling can be considered in the future in order to study the dynamic behaviour of a complex structure using minimal computational resources. Effect of rotation on the nonlinear beam can also be investigated.

Acknowledgements

The author thank Rolls Royce for providing the financial support for this project. The first author is grateful to the Engineering and Physical Sciences Research Council and Rolls-Royce plc for funding this work under the Industrial CASE Award scheme (Award No. 2155162).

Dr Loic Salles and Dr Fadi El Haddad thank Rolls-Royce plc and the EPSRC for the support under the Prosperity Partnership Grant "Cornerstone: Mechanical Engineering Science to Enable Aero Propulsion Futures", Grant Ref: EP/R004951/1.

The authors are grateful to Rolls-Royce plc for giving permission to publish it.

References

[1] M. Krack, L. Salles, and F. Thouverez, "Vibration prediction of bladed disks coupled by friction joints," *Archives of Computational Methods in Engineering*, vol. 24, no. 3, pp. 589–636, 2017.

[2] J. Bonet, A. J. Gil, and R. D. Wood, *Nonlinear solid mechanics for finite element analysis: statics*. Cambridge University Press, 2016.

[3] N. M. Krylov and N. N. Bogoliubov, *Introduction to non-linear mechanics*. Princeton University Press, 1949, no. 11.

[4] M. Urabe, "Galerkin's procedure for nonlinear periodic systems," WISCONSIN UNIV MADISON MATHEMATICS RESEARCH CENTER, Tech. Rep., 1964.

[5] T. Detroux, L. Renson, L. Masset, and G. Kerschen, "The harmonic balance method for bifurcation analysis of large-scale nonlinear mechanical systems," *Computer Methods in Applied Mechanics and Engineering*, vol. 296, pp. 18–38, 2015.

[6] T. Cameron and J. H. Griffin, "An alternating frequency/time domain method for calculating the steady-state response of nonlinear dynamic systems," 1989.

[7] Y.-L. Yeh, M.-J. Jang, and C. C. Wang, "Analyzing the free vibrations of a plate using finite difference and differential transformation method," *Applied mathematics and computation*, vol. 178, no. 2, pp. 493–501, 2006.

[8] K. Subrahmanyam and K. Kaza, "Vibration analysis of rotating turbomachinery blades by an improved finite difference method," *International journal for numerical methods in engineering*, vol. 21, no. 10, pp. 1871–1886, 1985.

[9] G. Kerschen, S. Shaw, C. Touzé, O. Gendelman, B. Cochelin, and A. Vakakis, *Modal analysis of nonlinear mechanical systems*. Springer, 2014, vol. 555.

[10] H. B. Keller, "Numerical solution of boundary value problems for ordinary differential equations: survey and some recent results on difference methods," in *Numerical solutions of boundary value problems for ordinary differential equations*. Elsevier, 1975, pp. 27–88.

[11] G. H. Meyer, *Initial value methods for boundary value problems: theory and application of invariant imbedding*. Academic Press, 1973.

[12] P. Pai and A. Palazotto, "Large-deformation analysis of flexible beams," *International Journal of Solids and Structures*, vol. 33, no. 9, pp. 1335–1353, 1996.

[13] M. Ahmadian, M. Mojahedi, and H. MOEINFARD, "Free vibration analysis of a nonlinear beam using homotopy and modified lindstedt-poincare methods," 2009.

[14] S. Chen, J. Huang, and K. Sze, "Multidimensional lindstedt–poincaré method for nonlinear vibration of axially moving beams," *Journal of Sound and Vibration*, vol. 306, no. 1-2, pp. 1–11, 2007.

[15] S. Song and A. Waas, "Effects of shear deformation on buckling and free vibration of laminated composite beams," *Composite Structures*, vol. 37, no. 1, pp. 33–43, 1997.

[16] H.-I. Yoon, I.-S. Son, and S.-J. Ahn, "Free vibration analysis of euler-bernoulli beam with double cracks," *Journal of mechanical science and technology*, vol. 21, no. 3, pp. 476–485, 2007.

[17] C. Wang, V. Tan, and Y. Zhang, "Timoshenko beam model for vibration analysis of multi-walled carbon nanotubes," *Journal of Sound and Vibration*, vol. 294, no. 4-5, pp. 1060–1072, 2006.

[18] S. Lin and K. Hsiao, "Vibration analysis of a rotating timoshenko beam," *Journal of Sound and Vibration*, vol. 240, no. 2, pp. 303–322, 2001.

[19] J. Lin, Z. Hu, Z.-S. Chen, Y.-M. Yang, and H.-L. Xu, "Sparse reconstruction of blade tip-timing signals for multi-mode blade vibration monitoring," *Mechanical Systems and Signal Processing*, vol. 81, pp. 250–258, 2016.

[20] M. Pan, Y. Yang, F. Guan, H. Hu, and H. Xu, "Sparse representation based frequency detection and uncertainty reduction in blade tip timing measurement for multi-mode blade vibration monitoring," *Sensors*, vol. 17, no. 8, p. 1745, 2017.

[21] P. Dash and B. Singh, "Nonlinear free vibration of piezoelectric laminated composite plate," *Finite Elements in Analysis and Design*, vol. 45, no. 10, pp. 686–694, 2009.

[22] N. S. Naidu and P. Sinha, "Nonlinear free vibration analysis of laminated composite shells in hygrothermal environments," *Composite Structures*, vol. 77, no. 4, pp. 475–483, 2007.

[23] X. Aubard, P.-A. Boucard, P. Ladevèze, and S. Michel, "Modeling and simulation of damage in elastomer structures at high strains," *Computers & structures*, vol. 80, no. 27-30, pp. 2289–2298, 2002.

[24] S. K. Sinha, "Combined torsional-bending-axial dynamics of a twisted rotating cantilever timoshenko beam with contact-impact loads at the free end," 2007.

[25] O. Weeger, U. Wever, and B. Simeon, "Nonlinear frequency response analysis of structural vibrations," *Computational Mechanics*, vol. 54, no. 6, pp. 1477–1495, 2014.

[26] M. Petyt, *Introduction to finite element vibration analysis*. Cambridge university press, 2010.

[27] A. Ben-Israel, "A newton-raphson method for the solution of systems of equations," *Journal of Mathematical analysis and applications*, vol. 15, no. 2, pp. 243–252, 1966.

[28] S. Whitney, "Vibrations of cantilever beams: Deflection, frequency, and research uses," *Website: Apr*, vol. 23, no. 10, 1999.

Appendix

A Finite Element Matrices

The shape function matrix $\mathbf{N}$ and matrices of derivatives of the shape function $\mathbf{B}_0$ and $\mathbf{B}_1$ are given by:

$$\mathbf{N}(\xi,\eta,\zeta) = \begin{bmatrix} N_1 & 0 & 0 & N_2 & 0 & 0 & ... & N_n & 0 & 0 \\ 0 & N_1 & 0 & 0 & N_2 & 0 & ... & 0 & N_n & 0 \\ 0 & 0 & N_1 & 0 & 0 & N_2 & ... & 0 & 0 & N_n \end{bmatrix} \tag{14}$$

$$\mathbf{B}_0(\xi,\eta,\zeta) = \begin{bmatrix} \frac{\partial N_1}{\partial x} & 0 & 0 & ... & ... & ... & \frac{\partial N_n}{\partial x} & 0 & 0 \\ 0 & \frac{\partial N_1}{\partial y} & 0 & ... & ... & ... & 0 & \frac{\partial N_n}{\partial y} & 0 \\ 0 & 0 & \frac{\partial N_1}{\partial z} & ... & ... & ... & 0 & 0 & \frac{\partial N_n}{\partial z} \\ 0 & \frac{\partial N_1}{\partial z} & \frac{\partial N_1}{\partial y} & ... & ... & ... & 0 & \frac{\partial N_n}{\partial z} & \frac{\partial N_n}{\partial y} \\ \frac{\partial N_1}{\partial z} & 0 & \frac{\partial N_1}{\partial x} & ... & ... & ... & \frac{\partial N_n}{\partial z} & 0 & \frac{\partial N_n}{\partial x} \\ \frac{\partial N_1}{\partial y} & \frac{\partial N_1}{\partial x} & 0 & ... & ... & ... & \frac{\partial N_n}{\partial y} & \frac{\partial N_n}{\partial x} & 0 \end{bmatrix} \tag{15}$$

$$\mathbf{B}_1(\mathbf{u}) = \mathbf{A}(u) \cdot \mathbf{G} \tag{16}$$

$$\mathbf{G} = \begin{bmatrix} \frac{\partial N_1}{\partial x} \otimes \mathbf{I}_3 & \frac{\partial N_2}{\partial x} \otimes \mathbf{I}_3 & ... & \frac{\partial N_n}{\partial x} \otimes \mathbf{I}_3 \\ \frac{\partial N_1}{\partial y} \otimes \mathbf{I}_3 & \frac{\partial N_2}{\partial y} \otimes \mathbf{I}_3 & ... & \frac{\partial N_n}{\partial y} \otimes \mathbf{I}_3 \\ \frac{\partial N_1}{\partial z} \otimes \mathbf{I}_3 & \frac{\partial N_2}{\partial z} \otimes \mathbf{I}_3 & ... & \frac{\partial N_n}{\partial z} \otimes \mathbf{I}_3 \end{bmatrix} \tag{17}$$

$$\mathbf{A}(u) = \begin{bmatrix} \frac{\partial u_x}{\partial x} & \frac{\partial u_y}{\partial x} & \frac{\partial u_z}{\partial x} & 0 & 0 & 0 & 0 & 0 & 0 \\ 0 & 0 & 0 & \frac{\partial u_x}{\partial y} & \frac{\partial u_y}{\partial y} & \frac{\partial u_z}{\partial y} & 0 & 0 & 0 \\ 0 & 0 & 0 & 0 & 0 & 0 & \frac{\partial u_x}{\partial z} & \frac{\partial u_y}{\partial z} & \frac{\partial u_z}{\partial z} \\ 0 & 0 & 0 & \frac{\partial u_x}{\partial z} & \frac{\partial u_y}{\partial z} & \frac{\partial u_z}{\partial z} & \frac{\partial u_x}{\partial y} & \frac{\partial u_y}{\partial y} & \frac{\partial u_z}{\partial y} \\ \frac{\partial u_x}{\partial z} & \frac{\partial u_y}{\partial z} & \frac{\partial u_z}{\partial z} & 0 & 0 & 0 & \frac{\partial u_x}{\partial x} & \frac{\partial u_y}{\partial x} & \frac{\partial u_z}{\partial x} \\ \frac{\partial u_x}{\partial y} & \frac{\partial u_y}{\partial y} & \frac{\partial u_z}{\partial y} & \frac{\partial u_x}{\partial x} & \frac{\partial u_y}{\partial x} & \frac{\partial u_z}{\partial x} & 0 & 0 & 0 \end{bmatrix} \tag{18}$$

$$\mathbf{G} \cdot \{\mathbf{a}_e\} = \begin{bmatrix} \frac{\partial u_x}{\partial x} & \frac{\partial u_y}{\partial x} & \frac{\partial u_z}{\partial x} & \frac{\partial u_x}{\partial y} & \frac{\partial u_y}{\partial y} & \frac{\partial u_z}{\partial y} & \frac{\partial u_x}{\partial z} & \frac{\partial u_y}{\partial z} & \frac{\partial u_z}{\partial z} \end{bmatrix} \tag{19}$$

B Formulation in Harmonic Balance Method and Continuation Scheme

B.1 Linear Matrix in Harmonic Balance Method

Details of $\mathbf{A}(\omega)$ matrix in the harmonic balance method equation (Equation 11):

$$\mathbf{A}(\omega) = \begin{bmatrix} \mathbf{K} & & & & & \\ & \mathbf{K}-\omega^2\mathbf{M} & \omega\mathbf{C} & & & \\ & -\omega\mathbf{C} & \mathbf{K}-\omega^2\mathbf{M} & & & \\ & & & \ddots & & \\ & & & & \mathbf{K}-(\omega N_H)^2\mathbf{M} & \omega N_H\mathbf{C} \\ & & & & -\omega N_H\mathbf{C} & \mathbf{K}-(\omega N_H)^2\mathbf{M} \end{bmatrix} \tag{20}$$

B.2 Continuation Scheme

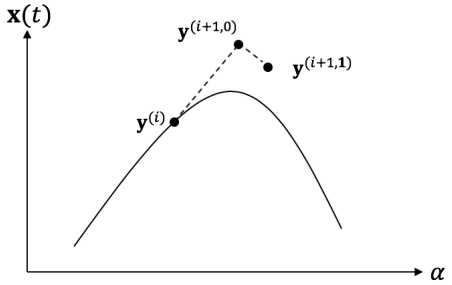

Figure 8: The prediction and correction step in the continuation scheme

Following notations as shown on Figure 8 are going to be used:

- $\mathbf{y}^{(i)} = (\mathbf{x}^{(i)}, \alpha^i)$: i-th converged point;
- $\mathbf{y}^{(i+1,0)} = (\mathbf{x}^{i+1,0}, \alpha^{(i+1,0)})$: prediction for $(i+1)$-th point;
- $\mathbf{y}^{(i+1,j)} = (\mathbf{x}^{(i+1,j)}, \alpha^{(i+1,j)}$: $(i+1)$-th point after j correction steps.

B.2.1 Prediction Method

To predict a point in the state-space, a direction and a distance is needed. The step size $\Delta s^{(i+1)}$ is the distance between the converged points $\mathbf{y}^{(i)}$ and the predict point $(\mathbf{x}^{(i+1,0)}, \alpha^{(i+1,0)})$. In Secant Method, two converged points in the previous step $(\mathbf{x}^{(i-1)}, \alpha^{i-1})$ and $(\mathbf{x}^{(i)}, \alpha^{(i)})$ are used to predict the point $(\mathbf{x}^{(i+1,0)}, \alpha^{(i+1,0)})$.

$$\Delta s^{(i+1)} = \sqrt{(\mathbf{x}^{(i+1)} - \mathbf{x}^{(i)})^T(\mathbf{x}^{(i+1)} - \mathbf{x}^{(i)}) + (\alpha^{(i+1)} - \alpha^{(i)})^2} \tag{21}$$

$$(\mathbf{x}^{(i+1,0)}, \alpha^{(i+1,0)}) = (\mathbf{x}^{(i)}, \alpha^{(i)}) + \Delta s^{i+1}\left((\mathbf{x}^{(i)}, \alpha^{(i)}) - (\mathbf{x}^{(i-1)}, \alpha^{i-1})\right) \tag{22}$$

B.2.2 Correction Method

The correction step in continuation scheme is used to move the predicted point $(\mathbf{x}^{(i+1,0)}, \alpha^{(i+1,0)})$ towards to the converged point $\mathbf{y}^{(i+1)}$ which satisfies Equation 11. In Arc Length Constraint, distance between the corrected points and the previous converged point is fixed. The arc-length method has the ability to pass turning points.

$$\forall j \geq 1, \quad \|\mathbf{x}^{(i+1,j+1)} - \mathbf{x}^{(i)}\|^2 + |\alpha^{(i+1,j+1)} - \alpha^{(i)}|^2 = (\Delta s^{(i+1)})^2 \tag{23}$$

C Newton Direction Computation for Harmonic Balance

1: Pre-assembly **M**, **C**, $\mathbf{K}_0$ matrices in Equation 6 and vector $\tilde{\mathbf{b}}_{ext}$.

2: Set tolerance ϵ_r

3: Initial Guess $(\omega_0, \tilde{\mathbf{q}}_0)$

4: Set $\omega = \omega_0$ and $\tilde{\mathbf{q}} = \tilde{\mathbf{q}}_0$

5: **REPEAT**

6: **for** $k = 0, \ldots, (N_t - 1)$ **do**

7: IDFT: $\mathbf{x}(t_k) = \frac{1}{2}\,\tilde{\mathbf{q}}^{0,c} + \sum_{n=1}^{N_H} \tilde{\mathbf{q}}^{n,c} \cdot \cos(\frac{2\pi}{N_t} \cdot k\,n) + \tilde{\mathbf{q}}^{n,s} \cdot \sin(\frac{2\pi}{N_t} \cdot k\,n)$

8: $\mathbf{x}(t_k) \rightarrow \mathbf{K}_{nl}$ and $\frac{\partial \mathbf{F}_{nl}}{\partial \mathbf{x}}(t_k)$

9: $\mathbf{K}_{nl} \rightarrow \mathbf{F}_{nl}(t_k)$

10: **end for**

11: $\mathbf{F}_{nl}(\mathbf{x}, t) \xrightarrow{DFT} \tilde{\mathbf{b}}_{nl}$

$\tilde{\mathbf{b}}_{nl}^{n,c} = \frac{2}{N_t} \times \sum_{k=0}^{N_t-1} \mathbf{F}_{nl}(t_k)) \cdot \cos(\frac{2\pi}{N_t} \cdot k\,n)$

$\tilde{\mathbf{b}}_{nl}^{n,s} = \frac{2}{N_t} \times \sum_{k=0}^{N_t-1} \mathbf{F}_{nl}(t_k)) \cdot \sin(\frac{2\pi}{N_t} \cdot k\,n)$

12: Compute $\mathbf{A}(\omega)$

13: $\mathbf{Z}(\omega, \tilde{\mathbf{q}}) \equiv \mathbf{A}(\omega)\tilde{\mathbf{q}} + \tilde{\mathbf{b}}_{nl}(\tilde{\mathbf{q}}) - \tilde{\mathbf{b}}_{ext} = 0$

14: Jacobian Matrix: $\frac{\partial \mathbf{F}_{nl}}{\partial \mathbf{x}}(t_k) \xrightarrow{DFT} \mathbf{Z}'$

15: Arc Length Constraint

16: Newton Direction Computation:

$\mathbf{Z}'(\omega, \tilde{\mathbf{q}}) \cdot \Delta = -\mathbf{Z}(\omega, \tilde{\mathbf{q}})$

$(\omega_1, \tilde{\mathbf{q}}_1) = \Delta + (\omega, \tilde{\mathbf{q}})$

17: Update: $\omega = \omega_1$ and $\tilde{\mathbf{q}} = \tilde{\mathbf{q}}_1$

18: Evaluate Residual: $r = \mathbf{Z}(\omega_1, \tilde{\mathbf{q}}_1)$

19: **UNTIL** $r \leq \epsilon_r$

20: Return value $(\omega, \tilde{\mathbf{q}})$

21: Predict next point with Secant Method

N_H is the total number of harmonics considered in HBM and N_t is the total number of samples taken per period for DFT and IDFT.

Step 6 to 11 correspond to procedure AFT in the flowchart shown in Figure 5. Step 12 to 13 correspond to assembly of $\mathbf{Z}(\omega, \tilde{\mathbf{q}})$, computation of Jacobian matrix $\mathbf{Z}'$ and Newton direction computation are shown in step 14 and 16 respectively.